Electrochimica Acta 536 (2025) 146718

Contents lists available at ScienceDirect

Electrochimica Acta

journal homepage: www.journals.elsevier.com/electrochimica-acta

A dual-signal sensor based on molecularly imprinted photonic polydopamine for detection of the oxidative stress biomarker allantoin

Akmaral Suleimenova [a,b], Ana C. Marques [b], Manuela F. Frasco [a,*], Elvira Fortunato [b], M. Goreti F. Sales [a,*]

[a] BioMark, CEMMPRE, ARISE, Department of Chemical Engineering, Faculty of Sciences and Technology, University of Coimbra, Coimbra, Portugal
[b] CENIMAT|i3N, Department of Materials Science, School of Science and Technology, NOVA University of Lisbon and CEMOP/UNINOVA, Caparica, Portugal

ARTICLE INFO

Keywords:
Dual-signal sensor
Molecularly imprinted polymer
Polydopamine
Structural coloration
Oxidative stress
Allantoin

ABSTRACT

A novel biomimetic detection method is presented allocating two transducer principles in a molecularly imprinted polymer (MIP)-based sensor. The device was constructed on a transparent three-electrode system of conductive indium tin oxide (ITO) fabricated by laser direct writing on glass substrates. The sensing layer was prepared by electropolymerizing dopamine in the presence of allantoin, on colloidal silica particles that exhibited a structural color due to the short-range ordered structure. This opto-electrochemical dual-signal output was successfully developed for the detection of the oxidative stress biomarker allantoin. The analytical properties were evaluated by electrochemical impedance spectroscopy and reflectance analysis of the structural color. The sensor showed a linear response over a wide range of allantoin concentrations (0.1 nmol L^{-1} to 10000 nmol L^{-1}) measured in synthetic urine. As expected, the lowest limit of detection in urine (0.012 nmol L^{-1}) was achieved with the electrochemical signal. In addition, other urinary oxidative stress metabolites tested as interferents, namely uric acid and 8-hydroxy-2′-deoxyguanosine, had no effect on the dual-signal detection of allantoin. The biomimetic and cost-effective properties of the materials in combination with the improved analytical properties of opto-electrochemical detection provide a sensor platform with great potential for the screening of oxidative stress biomarkers in urinalysis.

1. Introduction

New approaches based on dual-signal outputs usually combine opto-electrochemical responses [1], and the integration of biomimetic materials has only recently been pursued [2,3]. In terms of optical detection, bioinspired photonic structures are very attractive due to the tunability and low cost of achieving structural colors based on the self-assembly of colloidal particles. The most common biosensor designs are based on the fabrication of photonic polymers that respond to specific stimuli by wavelength shifting or intensity variations of the reflectance peak. The versatility of these materials has led to an increasing development of sensors based on photonic polymers [4,5]. In most cases, periodically organized structures that produce iridescent colors have been used to develop colorimetric sensors. However, the properties of quasi-ordered structures or amorphous colloidal arrays, which have short-range order and produce isotropic (angle-independent) colors, can be very interesting for sensor applications [3,6].

When using photonic crystals or polymer-based structural color materials combined with electric fields, most studies explore the possibility of nanostructures to improve the performance of photo-electrochemical devices [7,8], to enhance the switching contrast of electrochromic materials [9,10] or to follow color variations based on the electric-responsiveness of polymers [11,12]. As a convenient and efficient method to produce polymer films that adhere to the electrodes, electrochemical polymerization has been widely used in this context. Colloidal crystal sacrificial arrays can be first assembled on the electrodes to form porous inverse opal structures before or after electropolymerization and originate patterned or nanostructured polymer films [13,14]. However, the potential of one-step electropolymerization to produce structural color-based electrodes for dual-signal detection has never been explored, especially with biomimetic approaches based on molecularly imprinted polymers (MIPs).

Molecular imprinting is a mature technology that makes it possible to produce more cost-effective, stable, and robust bioreceptors than their

* Corresponding authors.
E-mail addresses: mffrasco@uc.pt (M.F. Frasco), maria.sales@uc.pt (M.G.F. Sales).

https://doi.org/10.1016/j.electacta.2025.146718
Received 10 February 2025; Received in revised form 13 June 2025; Accepted 14 June 2025
Available online 14 June 2025

biological counterparts [15,16]. MIPs form during the synthesis of polymeric materials in the presence of the target analyte and create selective recognition sites within the polymer network as unique cavities in shape and chemistry [17,18]. One of the best-known techniques for *in situ* MIP growth with precise control of the structure and thickness of the polymer formed is electropolymerization [19]. Intensive research has therefore been carried out on electrochemical sensors based on MIPs. The reason for this is the variety of polymers that can be produced, the simple electrochemical control of polymer formation and template removal, and the easy customization to a variety of target analytes, combining robustness and excellent detection capabilities [20].

In this work, for the first time, two transducer principles are combined in a MIP sensor to detect biomarkers of oxidative stress by simultaneous electrochemical impedance spectroscopy (EIS) and reflectance analysis of structural colors. The use of a single signal readout can lead to inaccuracies. Therefore, several studies have shown that the same receptor can be combined with different transducer principles. In particular, the dual-signal modes have increased the sensitivity, reliability and stability of the sensors [21–23]. The developed sensor was used as a proof-of-concept for the detection of the oxidative stress metabolite allantoin. Allantoin is the main product of the non-enzymatic oxidation of uric acid by free radicals. Its content in urine is stable and does not correlate with uric acid levels. Therefore, allantoin levels have been used to measure oxidative status in the context of various diseases [24–27].

Although allantoin is considered a biomarker for oxidative stress, there are few biosensors for its detection, and most methods rely on liquid chromatography-mass spectrometry and chemiluminescence techniques [27–30]. All previous methods are therefore still very laborious, expensive, and time-consuming. Therefore, a relatively simple, cheap and precise method for the quantification of allantoin in urine would enable a broad application for the monitoring of oxidative stress.

The sensor was assembled on indium tin oxide (ITO) glass, which is a suitable platform for detecting both electrochemical and optical signals due to its transparency and conductivity [31,32]. To construct the sensor, the MIP sensing layer was fabricated *in situ* by electropolymerization of dopamine in the presence of colloidal silica particles whose presence on the surface exhibited a short-range structural color. This approach is also known as surface imprinted polymer, as the imprinted sites that can lead to binding positions are obtained on the outer layer of polydopamine (PDA). PDA is a widely studied biopolymer for surface coating, synthesis of MIPs and fabrication of photonic crystal structures, utilizing some of its interesting properties such as adhesiveness, conductivity and black granules that absorb scattered light [33–37]. The demonstrated sensitivity and stability properties of the dual detection method are very promising and thus offer significant advantages as a label-free, simple, and cost-effective sensing solution.

2. Materials and methods

2.1. Chemicals

Potassium ferrocyanide ($K_4[Fe(CN)_6]\cdot 3H_2O$), potassium ferricyanide ($K_3[Fe(CN)_6]$) and dipotassium hydrogen phosphate were bought from Riedel-de-Häen; 3-hydroxytyraminium chloride, tetraethylorthosilicate (TEOS) 99%, calcium chloride dihydrate and Extran® MA-01 were purchased from Merk; Allantoin, uric acid, 8-hydroxy-2′-deoxyguanosine (8-OHdG), citric acid, and absolute ethanol were obtained from Sigma-Aldrich; Ammonium hydroxide 25%, DL-lactic acid and creatinine were obtained from Fluka; Sodium hydrogen carbonate, sodium chloride, magnesium sulfate heptahydrate, potassium dihydrogen phosphate, hydrochloric acid and ammonium chloride were acquired from Panreac; Phosphate Buffer Saline (PBS) tablets were from Amresco; Urea was purchased from Fagron. All reagents were of analytical grade and used as acquired without further purification. Solutions were prepared using ultrapure laboratory grade water (conductivity $< 0.06\mu S\ cm^{-1}$).

2.2. Preparation of indium tin oxide (ITO) electrodes

The 3-electrode system was prepared on commercially available ITO coated glass substrates by direct laser writing technique. The electrodes were designed as represented in Fig. 1A; these were obtained on glass substrates, by a pulsed CO_2 infrared laser cutting system (Universal Laser System VLS 3.5), with a focal length of 50.8 mm, wavelength of 10.6 μm and 2.0" lens (focus point of 0.127 mm). The laser was operated at 35 W, 1000 pulses per inch and a scanning rate of 1.27 m/s. Before biosensor assembly, ITO electrodes were thoroughly washed with Extran® MA-01 solution, ultrapure water and dried under nitrogen flow.

2.3. Synthesis of colloidal silica particles

Monodisperse spherical colloidal silica particles were synthesized using a modification of the Stöber method [38]. Two solutions were prepared at room temperature. Solution A was obtained by mixing ammonia (1.8 mol L^{-1}) and ethanol (3 mol L^{-1}) in ultrapure water, and solution B consisted of mixing ethanol (7.8 mol L^{-1}) with TEOS (0.2 mol L^{-1}). Both solutions were added together, mixed under vigorous stirring, and then the reaction occurred for 2 h at 25 °C at 250 rpm. After the synthesis, the colloidal suspension was cleaned by several rounds of centrifugation at 9000 rpm and final resuspension in ultrapure water.

2.4. Biosensor assembly

The structural color MIP was assembled on the ITO working electrode (WE) by electropolymerization of dopamine in the presence of silica spherical particles and the target allantoin molecule, using as pseudo-reference electrode the smallest electrode that also contained ITO. Briefly, 160 μL of silica suspension (1.25 wt% in water) was centrifuged and separated from supernatant followed by addition of 60μL of 20 mmol L^{-1} allantoin in PBS buffer (0.01 mol L^{-1}, pH 6) and mixing for 10 min. Then, 60μL of 16 mmol L^{-1} dopamine in PBS buffer (0.01 mol L^{-1}, pH 6) was added and mixed for another 10 min. This suspension (60 μL) was placed on the ITO electrodes and the electropolymerization was performed by cyclic voltammetry (CV), 20 cycles in a range between +0.7 to +1.2 V, and scan rate of 50 mV/s. Then, electrodes were carefully washed with ultrapure water and dried under nitrogen flow. For template removal, the constructed biosensors were incubated overnight with ultrapure water to remove the imprinted allantoin, due to its strong solubility in water [39]. As control, a structural color non-imprinted polymer (NIP) was constructed using a similar procedure but without allantoin.

2.5. Analytical performance of dual-signal sensor

The analytical performance of the biosensor was evaluated through the rebinding properties of allantoin molecules after stabilization in PBS buffer (0.01 mol L^{-1}, pH 6). Calibration curves were obtained by incubating the WE with increasing allantoin concentrations (0.1 nmol L^{-1} to 10000 nmol L^{-1}) prepared in PBS buffer (0.01 mol L^{-1}, pH 6) for 30 min, on the same electrode unit. After each incubation, electrodes were carefully rinsed with ultrapure water, dried under nitrogen flow, and measured to obtain electrochemical and reflectance spectra, as described below. Both methods are used to assess the overall biosensor performance in terms of linear range and limit of detection (LOD). The biosensors prepared with the NIP were also evaluated as control.

To simulate the effect of close to real biological conditions, sensor responses were also evaluated with the same range of allantoin concentrations (0.1 nmol L^{-1} to 10000 nmol L^{-1}) prepared in 50-fold diluted synthetic urine and incubated for 30 min in the WE to establish the calibration curve in this condition. Synthetic urine was prepared according to the literature and contained creatinine, urea, DL-lactic

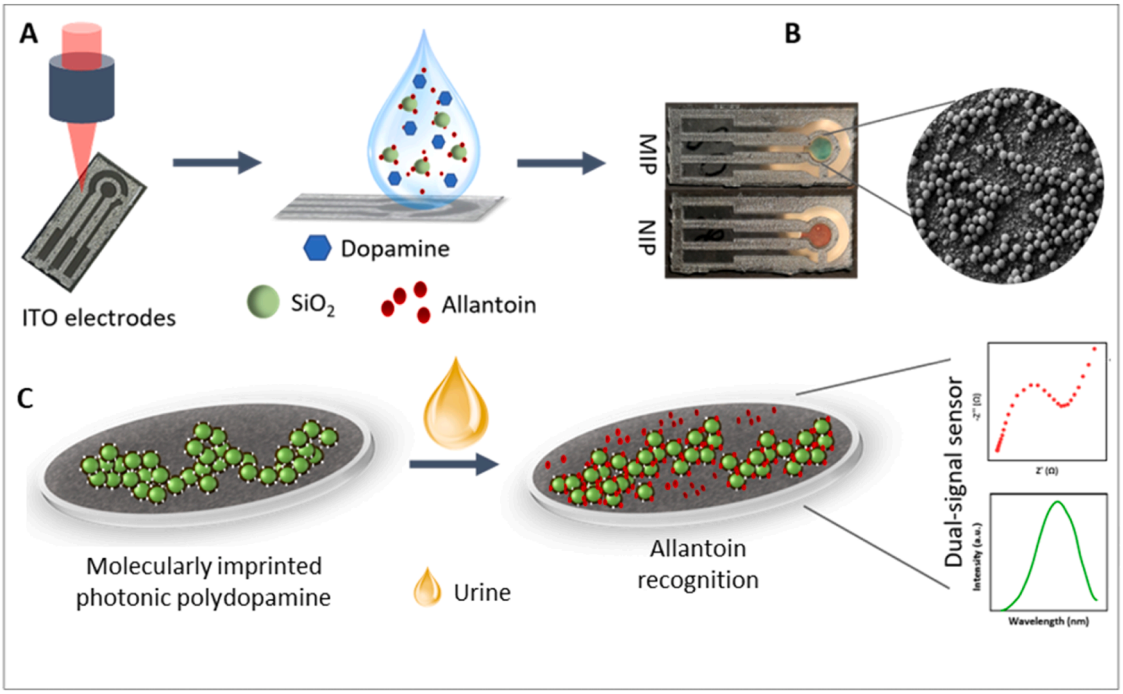

Fig. 1. Sketch of the sensor concept, showing the fabrication of ITO electrodes by direct laser writing technique (A), followed by MIP preparation, showing the structural colors obtained on the working electrodes of MIP and respective NIP control (B) to obtain the dual-signal sensors to detect allantoin by opto-electrochemical measurements (C).

acid, citric acid, ammonium chloride, magnesium sulfate, sodium chloride, calcium chloride, sodium hydrogen carbonate, potassium dihydrogen phosphate and dipotassium hydrogen phosphate at pH 6 [40]. All analytical results are expressed as the mean± standard deviation from at least three independent replicas (i.e., separate electrodes) per experiment. Bland-Altman analysis was performed to assess the agreement between the electrochemical and optical methods. The differences between the two methods were plotted against their mean values, and the bias, standard deviation, and 95% limits of agreement were calculated for both buffer and urine matrices [41].

Aiming to determine the applicability of the sensor, further recovery assays were performed by spiking 50-fold diluted urine with two known concentrations of allantoin (1 nmol L^{-1} and 35 nmol L^{-1}). In addition, the sensor response was analyzed against competing interfering oxidative stress metabolites that could be present in urine, namely uric acid and 8-OHdG [42–45]. For this, 50-fold diluted urine was spiked with the two known concentrations of allantoin (1 nmol L^{-1} and 35 nmol L^{-1}) combined with uric acid (0.1 mmol L^{-1}) or with 8-OHdG (71 nmol L^{-1}). Each solution was incubated for 30 min, the same period used in the calibration procedure.

2.5.1. Electrochemical measurements

Calibration curves were analyzed electrochemically by EIS measurements made in open circuit potential using a sinusoidal potential perturbation with 0.01 V of amplitude and 50 frequency values logarithmically distributed over a frequency range from 0.01 Hz to 100 kHz. The EIS assays were performed using 5.0×10^{-3} mol L^{-1} of $[Fe(CN)_6]^{3-}$ and 5.0×10^{-3} mol L^{-1} of $[Fe(CN)_6]^{4-}$ as redox probe, prepared in PBS buffer (0.01 mol L^{-1}, pH 6). Sensor responses were analyzed by relative charge transfer resistance (R_{ct}), i.e. $\Delta R_{ct}/R^0_{ct}$, where ΔR_{ct} is the difference between the R_{ct} obtained for each allantoin standard and the R^0_{ct} value obtained for the blank. Calibration plots were then depicted as $\Delta R_{ct}/R^0_{ct}$ against the logarithm concentration of allantoin to evaluate the response with regard to the linear regression obtained. The LOD was calculated as the concentration taken at the point of intersection of the fitted linear curve (at the minimum 95% confidence limit) and a line parallel to the x-axis through the mean intensity value measured in the lowest concentration [46].

2.5.2. Optical measurements

Simultaneously, the ability to recognize increasing amounts of allantoin was evaluated optically, based on the alterations induced in the reflectance spectra of the short range ordered structure of silica particles and plotting the calibration curve. Data regarding optical sensor responses was analyzed by relative intensity, i.e.,$\Delta I/I^0$, whereΔI is the difference between the maximum intensity of the peak and the I^0 maximum peak intensity of the control spectrum without allantoin. As for the electrochemical measurements, calibration plots of optical signal ($\Delta I/I^0$) against the logarithm concentration of allantoin were used to determine the LOD by following IUPAC procedure for logarithmic dependent calibrations [46].

2.6. Apparatus and characterization

Scanning Electron Microscopy (SEM) images were collected with a Carl Zeiss AURIGA CrossBeam SEM-FIB microscope, operating with a voltage of 5 kV. The electrochemical measurements were performed using a PalmSens4 potentiostat / galvanostat / impedance analyzer controlled by PSTrace 5.5 software. The optical measurements were performed with spectrophotometer having a reflection fiber probe (diameter 200 μm, DropSense) and deuterium-halogen light source (Metrohm, AG). A diffuse reflectance standard was used as a reference surface and the reflectance was collected at 90º incidence.

3. Results and discussion

3.1. Design and characterization of the biosensor assembly

The scheme of the dual-signal sensor is depicted in Fig. 1, which corresponds to an optimized version of several development stages of the biosensor. Considering that this work is a combination of photonic structures modified by electrochemical action on a conductive substrate,

the degree of novelty is high, and the difficulties found were numerous. Therefore, it is important to point out that this work used different experimental setups and materials that had been previously tested. In the first approach of this work, another polymer was used, which was subjected to several optimization steps, including the concentration of the monomer, the solvents used for the polymerization stage, the CV scanning conditions, and silica particles (concentration and deposition). After many experiments, only the best configuration reached is described in this work.

Overall, the first step of sensor design was to use commercial ITO glass to fabricate a 3-electrode system by direct laser writing technique. In this method, the ITO layer is etched to obtain the designed setup (Fig. 1A), where the conductive ITO layer was responsible for the final shape of the 3-electrode system. It is important to note that the ITO layer that remains on the glass is the one responsible for the format of the electrodes and was the part of the ITO surface that was not removed by the laser beam. It can therefore be assumed that the ITO electrodes are made of the same ITO material as the commercially available one. Thus, the ITO layer having no laser impact is expected to have similar XPS spectra to those reported in the literature (e.g [47]), which can also depend on the cleaning method (e.g [48]). What was important here, however, was that the shape of the ITO electrodes obtained corresponded to expectations, which was confirmed by the eye when reflecting light and by the generation of an electrochemical signal.

Then, previously synthesized silica particles were mixed with the allantoin target biomarker and dopamine and cast on the electrodes. At the assayed conditions, positive amino groups of allantoin are expected to form electrostatic interactions with negatively charged silica particles and the oligomers of dopamine around the system. This mixture was then electropolymerized on the surface of the ITO WE, with the expectation of creating a conductive PDA matrix with short-range ordered silica particles, conferring structural color to the WE (Fig. 1B). After allantoin removal from the polymer, imprinted sites remain for the selective recognition of the biomarker, which can be followed both electrochemically and optically (Fig. 1C).

The silica particles are expected to have a thin shell of PDA that serves also as an adhesive coating to link the particles to the electrode surface. The choice of dopamine as monomer was based on the well-known bioinspired adhesive properties of PDA, ease of synthesis, stability, and biocompatibility. In addition, the PDA layer can form an electrically conductive film on the ITO system [35,49].

Several studies were performed to optimize the PDA synthesis into an optimal film thickness in the ITO WE surface and to attach the silica particles to form a short-range structural color. The most suitable condition for successful PDA electropolymerization by CV was experimentally settled between +0.7 and +1.2 V by performing 20 cycles. CV analysis showed a polymerization peak at +1.09 V in the first cycle and then a rapid decrease in current with subsequent continuing increasing number of cycles (Fig. 2A). After 6 cycles, the current density of the oxidation peak started to reduce with lower differences from one cycle to another, confirming the formation of PDA film. It is important to note that the conductivity of PDA depends on the conditions in which electropolymerization is conducted. Herein, this was made in PBS buffer at nearly neutral pH. As such, the obtained PDA does not contribute to increasing the current of the electrochemical set-up under CV analysis. However, the possibility of a passivation layer being formed in this context cannot be ruled out.

The chemical modifications taking place at the surface of the electrode upon PDA formation were followed using EIS, monitoring the electron transfer properties of the surface against an iron-based redox probe. The EIS data were analyzed by Nyquist plots, showing the frequency response of the electrode-electrolyte system and area plot of the imaginary component (Z'') of the impedance against the real component (Z'). The R_{ct} at the electrode surface is given by the semicircle diameter obtained in EIS and can be used to define the interfacial properties of the electrode. Overall, the Nyquist plots showed that the R_{ct} values decreased after PDA formation, in comparison to bare ITO (Fig. 2B). For improved interpretation of the impedance response, the Nyquist plots are also presented with normalized scaling (equal x and y axes) (**Figure S1**). This occurred after assembling the MIP based on PDA or the NIP, acting as control, suggesting that the PDA film improved the conductive properties of the system suitable for subsequent electrochemical detection of allantoin, despite the presence of silica particles and allantoin. However, since consecutive scanning of the dopamine solution led to a decrease in current values in the CV, this result from the EIS could be related to the increased surface area generated by the presence of silica particles, expectedly covered by the PDA film.

It was interesting to note that the optical properties of the sensing layer of the NIP and the MIP were very different, with the electrodes displaying a different color (Fig. 1B). The fact that allantoin is present among the dopamine matrix that undergoes polymerization is expected to have several impacts upon the polymer being formed and the distribution of the silica particles. First, it is expected that allantoin decreases the rate of polymerization of dopamine, as it acts as an obstacle to the propagation of the growing chains. Second, allantoin (only present in the MIP) may establish electrostatic interactions with silica particles and dopamine due to opposite charges present, thereby leading to changes in the distribution of the particles on the surface of the electrode. As such, it is expected that the MIP films have silica particles closer to each other and lower amount of PDA, when compared to the NIP.

Thus, further analysis by SEM was pursued to monitor structural features that could confirm this (Fig. 3). The SEM images of silica particles (alone) showed their ability to self-assemble on substrates forming close-packed arrangements (Figs. 3A and 3B). In addition, it

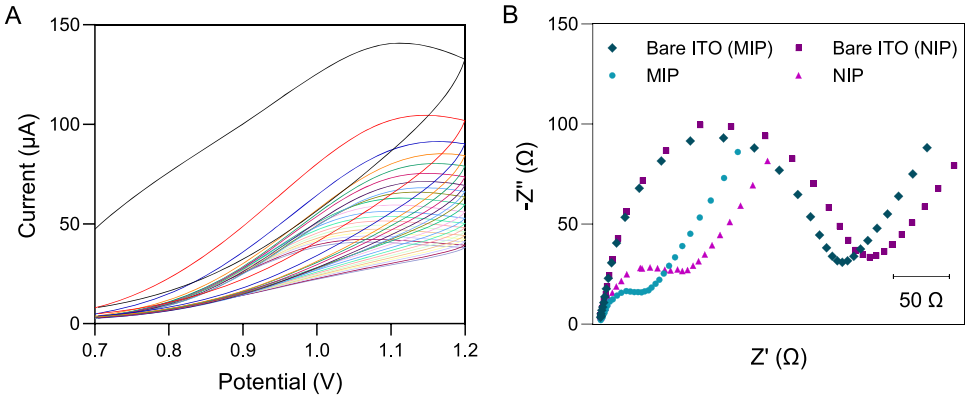

Fig. 2. Construction of biomimetic sensing films on ITO electrodes: (A) CV data during electropolymerization of dopamine (20 CVs between +0.7 and +1.2 V, scan rate 50 mV/s, using ITO as pseudo-reference); (B) Nyquist plots (0.01 Hz to 100 kHz) before and after electropolymerization of dopamine, i.e. bare ITO electrodes and after assembly of MIP and the NIP control, respectively, obtained in a solution of 5.0 mmol L^{-1} iron redox probe prepared in PBS buffer (0.01 mol L^{-1}, pH 6).

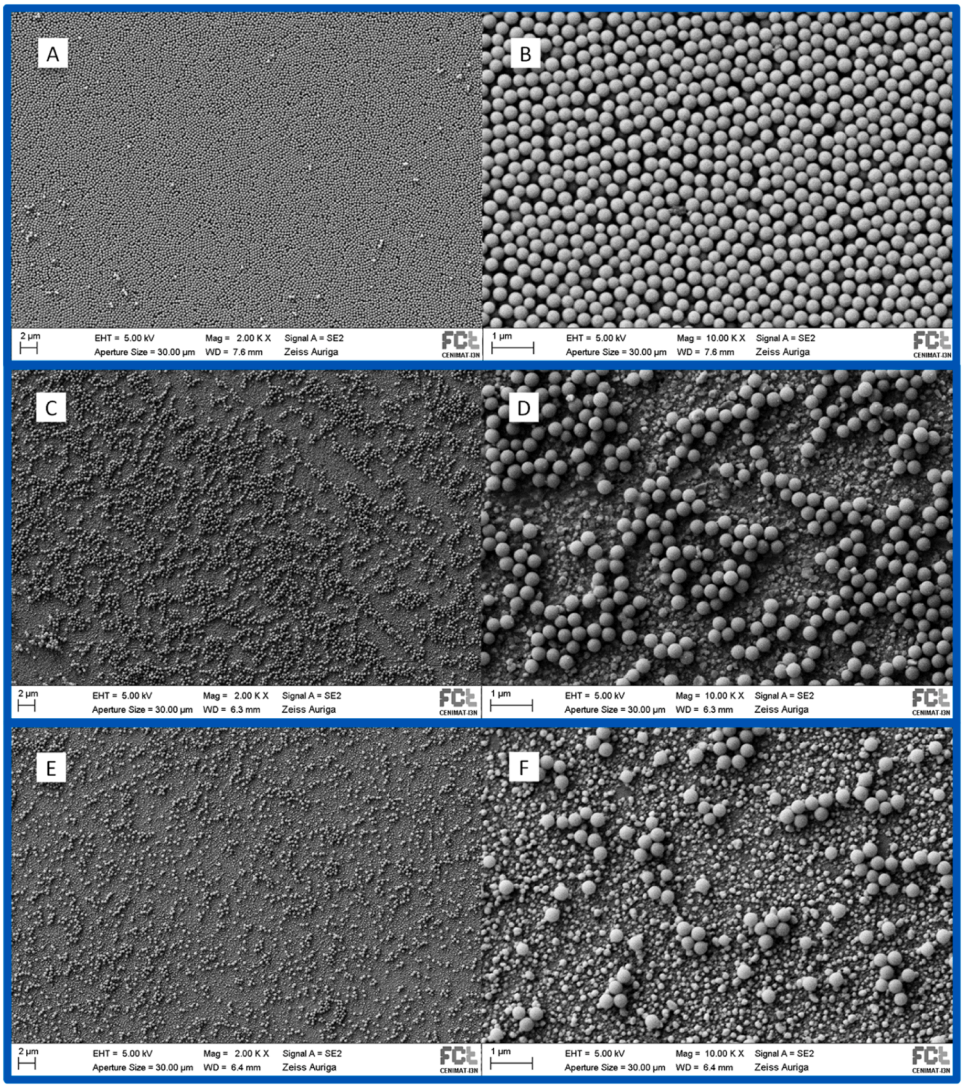

Fig. 3. Analysis by SEM of the (A, B) silica particles, (C, D) MIP assembled on ITO electrode, and (E, F) NIP assembled on ITO electrode.

demonstrated the expected spherical shape of the particles with an average diameter of 200 nm and confirmed the homogenous distribution of these particles in terms of size and spatial distribution. After constructing the sensor, the formation of the PDA film on the electrode is evident in the SEM images. The polymerization of dopamine results in small clusters of nanoparticles and a thin film embedding the silica particles (Figs. 3C – 3F), which altogether increased the surface area of the WE. The formation of PDA coatings on a variety of nanomaterials and colloids is well-described in the literature [36,37]. The presence of allantoin during MIP fabrication seemed to enable the assembly of a higher number of silica particles on the electrode surface (Figs. 3C and 3D) in comparison to the NIP control (Figs. 3E and 3F). This confirmed that the electrostatic interactions between the amine groups of dopamine surrounding the particles and the several electronegative elements in allantoin could reduce the repulsion forces between the particles, resulting in a more compact arrangement on the surface of the electrode. This observation is in agreement with the observed color on the WE, greenish with yellow hues in MIP and pale red in NIP (Fig. 1B). The SEM images also showed that the particles formed irregular interparticle spacing photonic structures, resulting in short-range structural colors [50]. As the MIP layer shows a higher number of silica particles with smaller interparticle distance, the maximum spectral reflectance appears on shorter wavelengths in comparison to NIP.

3.2. Detection of allantoin by electrochemical response

The analytical features evaluated were first monitored by electrochemistry, testing the response of both MIP and NIP sensors to increasing concentrations of allantoin and following the corresponding EIS response in the form of Nyquist plots. The obtained data was then used to plot the corresponding calibration curves. Overall, the obtained Nyquist plots showed a positive correlation between successive increase in allantoin concentration and the increase in R_{ct} (Fig. 4A), while the variation was random in NIP (Fig. 4B). For improved interpretation of the impedance response, the Nyquist plots are also presented with normalized scaling (equal x and y axes) (**Figure S2**). In the MIP, the results indicate that the resistance to charge transfer, i.e. the diameter of the semicircles in the Nyquist plots, increases in a concentration-dependent way; the higher the allantoin concentration, the higher the R_{ct}, following a linear trend against the log concentration. Thus, this R_{ct} increase confirms that allantoin is being recognized preferentially by the selective binding sites present in the MIP, which in turn hinders the access of the redox probe to the electrode surface and increases the resistance to charge transfer. This selective binding of allantoin to the MIP film is further supported by the random variations of the NIP, where there are no selective binding sites (because the polymer was obtained in the absence of allantoin). The lack of a clear trend in the NIP confirms that the signal increase in the MIP is not due to nonspecific adsorption or

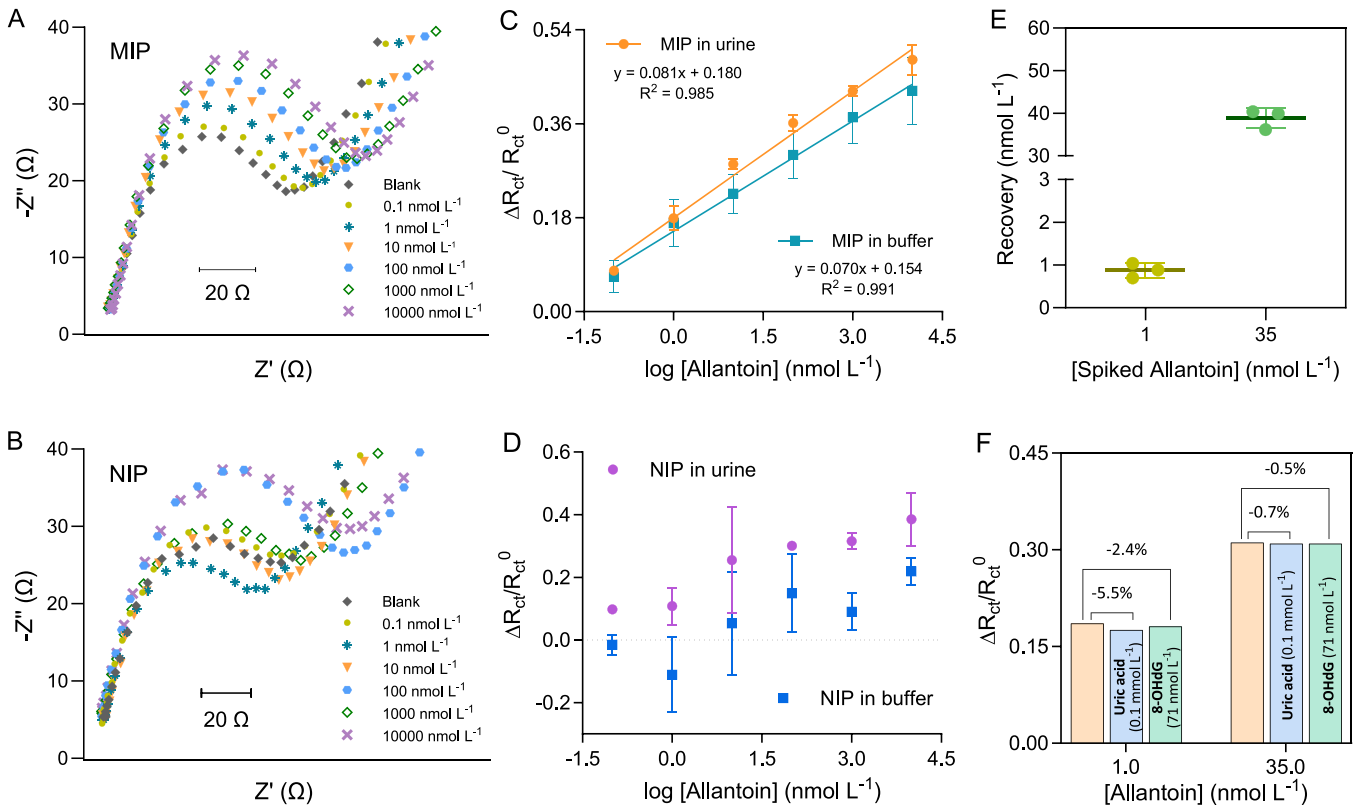

Fig. 4. Electrochemical analysis of the sensor response. Representative Nyquist plots (0.01 Hz to 100 kHz) of MIP (A) and NIP (B), in a solution of 5.0 mmol L^{-1} iron redox probe prepared in PBS buffer (0.01 mol L^{-1}, pH 6), and corresponding calibration curves in PBS buffer and synthetic urine of the MIP (C) and respective control NIP fluctuations (D). Recovery assays using MIP sensor after spiking urine with 1 and 35 nmol L^{-1} of allantoin (E). Interference studies by analyzing MIP response to allantoin in the presence of uric acid (0.1 mmol L^{-1}) and 8-OHdG (71 nmol L^{-1}) (F).

background effects, but rather to the selective interaction between the imprinted sites and allantoin.

This behavior was similar both in PBS buffer and synthetic urine, and the sensor showed a linear response in the concentration range tested (0.1 nmol L^{-1} to 10000 nmol L^{-1}) (Fig. 4C). In PBS buffer, a square of the correlation coefficient of 0.991 was obtained with an average slope of 0.070 (standard error of the slope of 0.3%). The obtained LOD in PBS buffer was 0.019 nmol L^{-1}. In 50-fold diluted synthetic urine, the square of the correlation coefficient was 0.985 with an average slope of 0.081 (standard error of the slope of 0.5%). The obtained LOD was 0.012 nmol L^{-1}. The analysis in synthetic urine correlated well with the one performed in simple PBS buffer medium, and the slightly higher LOD may reflect the ionic content of urine. In contrast, the NIP control showed random variations both in buffer and urine (Fig. 4D), demonstrating that the selective recognition sites in MIP were crucial for the observed sensor response. All these results were obtained by performing calibrations with at least three independent biosensors, confirming the reproducibility of the system in both conditions.

The accuracy of the system was monitored by means of recovery assays. The recovery studies were conducted by spiking 50-fold synthetic urine with known concentrations of allantoin (1.0 nmol L^{-1} and 35 nmol L^{-1}). Regarding the lowest concentration of 1.0 nmol L^{-1}, the measured value shifted -12.5% of the theoretical concentration with a relative standard deviation (RSD) of 19.6% (n = 3), while for the highest value of 35 nmol L^{-1} the shift was 10.9% with RSD of 6.0% (n = 3) (Fig. 4E). Thus, the measured values were consistent with the spiked levels suggesting an accurate determination of allantoin within the concentration range under analysis.

The selectivity of the system was tested by monitoring the response of the sensor to allantoin in the presence of other oxidative stress biomarkers that could act as interfering species in urine samples. Tests were conducted in 50-fold diluted synthetic urine against uric acid and 8-OHdG. Uric acid is an oxidative stress biomarker present in the urine, and it was chosen because allantoin is a product of uric acid oxidation [50]. In addition, uric acid as a precursor is a compound that has a similar structure to allantoin and could be recognized by the polymer matrix, which could interfere with the detection of allantoin. Another relevant oxidative stress metabolite is 8-OHdG, which is a major product of oxidative DNA damage and whose increased levels in urine have been used to detect oxidative stress [42,51,52]. The analysis of the R_{ct} values showed that the bias estimation varied between -0.7% and -5.5% for uric acid and between -0.5% and -2.4% for 8-OHdG (Fig. 4F). These results suggest that under the assayed conditions, uric acid and 8-OHdG did not interfere with the MIP response to allantoin. Considering the results obtained, a good applicability of the biosensor using the electrochemical response is expected.

3.3. *Detection of allantoin by optical response*

The procedures for evaluating the optical responses were similar to those described for the electrochemical system, as both signals were read sequentially after incubation with the target analyte. Therefore, the results were similarly obtained by performing calibrations with at least three independent biosensors. First, after incubating the sensor with the increasing allantoin concentrations, the optical signal was followed by changes in the reflectance spectra, which consequently generated calibration curves. The typical reflectance spectra obtained showed that an increase in the signal can be correlated positively with increasing concentrations of allantoin (Fig. 5A). The presence of increasing concentrations of allantoin occupying the binding sites on the MIP-PDA could decrease incoherent scattering resulting in increased color saturation. Similarly to electrochemical data, the intensity of the reflectance peak in

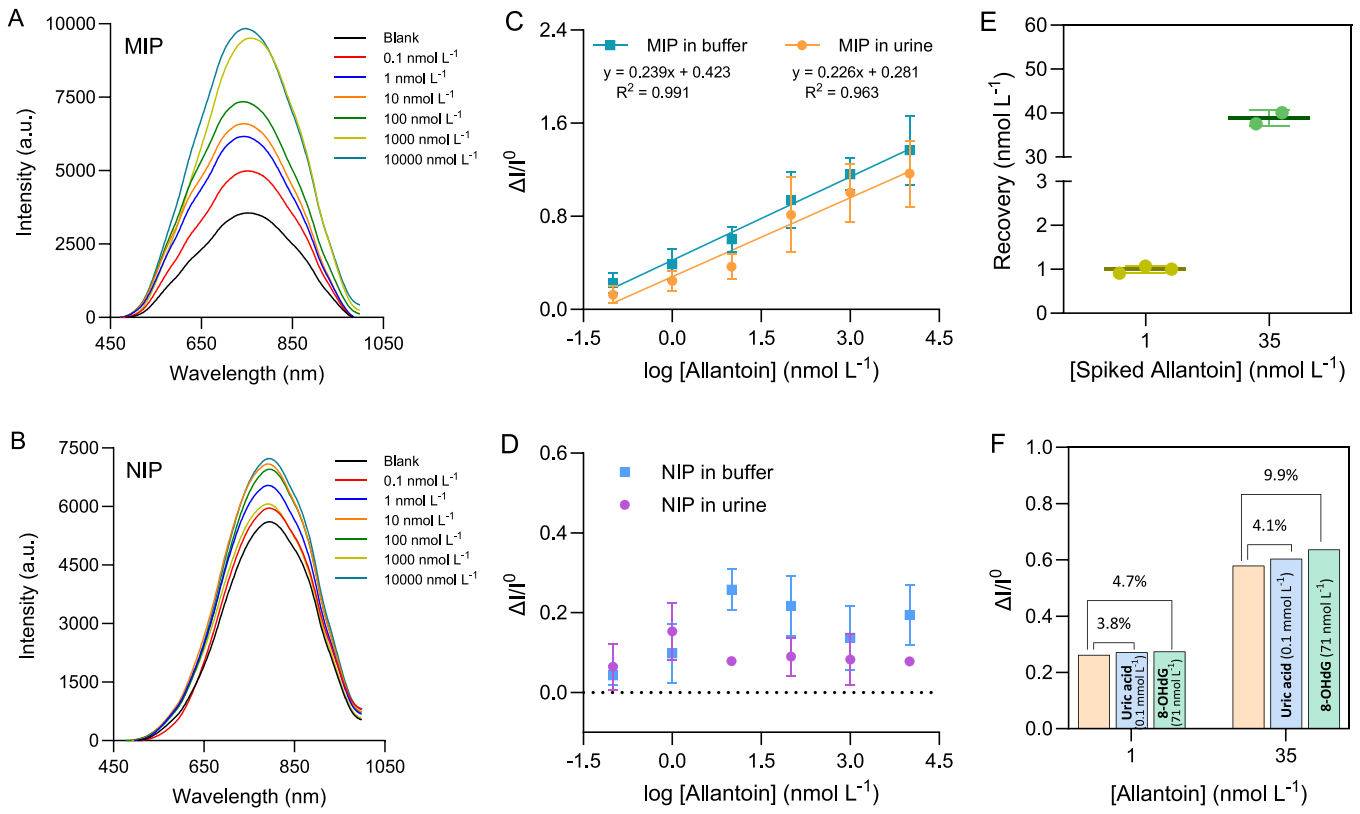

Fig. 5. Optical analysis of the sensor response: Representative reflectance spectra of MIP structural color materials (A) and respective NIP control (B) in PBS buffer and corresponding calibration curves of MIP sensor in PBS buffer and urine (C) and the NIP fluctuations (D); Recovery assays using MIP sensor after spiking urine with 1 and 35 nmol L^{-1} of allantoin (E); Interference studies by analyzing MIP response to allantoin in the presence of uric acid (0.1 mmol L^{-1}) and 8-OHdG (71 nmol L^{-1}) (F).

NIP control was random (Fig. 5B). In agreement with the observed structural color, the peaks in MIP were larger and shifted to the left of the visible spectra in comparison to NIP controls. The linear range was similar both in PBS buffer and synthetic urine (Fig. 5C). In PBS buffer, an average slope of 0.239 (standard error of the slope of 1.1%) with a square of the correlation coefficient of 0.991 was obtained. The calculated LOD in PBS buffer was 0.058 nmol L^{-1}. In 50-fold diluted synthetic urine, the square of the correlation coefficient was 0.963 with an average slope of 0.226 (standard error of the slope of 2.2%). The obtained LOD was 0.022 nmol L^{-1}. However, the analysis in synthetic urine showed higher variability in comparison to PBS buffer, as shown by the lower correlation coefficient. Lower LOD values were obtained with the electrochemical signal, but the optical response was also consistent to obtain useful results. As expected, the NIP control showed random variations both in buffer and urine (Fig. 5D).

The recovery studies by spiking 50-fold synthetic urine with the known concentrations of allantoin presented a shift of -0.28% with RSD of 8.1% (n = 3) regarding the lowest concentration of 1 nmol L^{-1}, and a shift of 10.9% with RSD of 4.5% (n = 2) for the highest value of 35 nmol L^{-1} (Fig. 5E). An accurate quantification of allantoin is also expected through the optical signal because the measured values were consistent with the spiked theoretical concentrations. Regarding the interference tests, the estimated bias for uric acid varied between 3.8% and 4.1% and for 8-OHdG a variation between 4.7% and 9.9% was obtained (Fig. 5F). These results are consistent with the higher optical signal variation when calibrating the sensor in urine, and these metabolites are not expected to alter the selective response to allantoin.

3.4. Optical versus electrochemical responses

The results confirmed that both optical and electrochemical responses are of analytical interest, as a linear trend is displayed in both when the MIP material is analyzed. The allantoin is binding preferentially to selective binding sites, because the behavior of the NIP is consistently random. The range of concentration yielding a linear response of the MIP is the same in both optical and electrochemical detection schemes, ranging from 0.1 to 10000 nmol L^{-1}. However, the electrochemical response seems to be more reproducible and less affected by urine components than the optical response, because it leads to calibration curves with correlation coefficients closer to one.

A Bland-Altman analysis was performed to compare electrochemical and optical methods. As shown in **Figure S3**, a bias was observed between the two methods, with an increasing trend in the difference as the concentration increases. This suggests that, when the electrochemical method is used as reference, the optical measurements tend to underestimate values at higher concentrations. The bias was calculated as -0.521 with a standard deviation of 0.319 and the 95% limits of agreement ranged from -1.15 to 0.104 for the buffer solution (**Figure S3A**). For the urine matrix, the bias was -0.319 with a standard deviation of 0.287 and the 95% limits of agreement ranged from -0.881 to 0.243 (**Figure S3B**). Notably, the best agreement between the two methods was observed at the lowest concentrations in the urine matrix. Importantly, no data points fell outside the 95% limits of agreement, suggesting that both methods exhibit good agreement across both matrices. Overall, while there is a small systematic bias, the two methods demonstrate reasonable consistency in their measurements.

The electrochemical response also leads to lower LODs, although the LOD values from electrochemical and optical assays are not significantly different from a clinical perspective. In terms of selectivity, the response of optical and electrochemical systems is similar, although this behavior may not be extended to other interfering species, especially when higher concentrations and components with intrinsic color are tested.

Overall, the capacity to operate with the same sensing layer and read in signals of different nature in the same spot (optical and electrochemical) has been confirmed. This approach is expected to contribute to more robust and accurate readings when real samples are considered, because any negative impact of the sample upon electrical readings is not expected to be the same (or of the same magnitude) when optical signals are collected.

4. Conclusions

This study provides new insights into the development of innovative biomimetic dual-signal opto-electrochemical sensors for the detection of biomarkers circulating in biological fluids. The designed sensor was prepared in a straightforward approach by electropolymerization of a dopamine solution with colloidal silica particles on transparent ITO glass electrodes. In this way, it takes advantage of the biocompatible and selective PDA MIP, which simultaneously produces a sensitive electrochemical responsive layer and a short-range structural color for dual signal measurements. The sensor detected allantoin in a wide linear range and it was possible to achieve low LODs. Furthermore, the response of the sensor material to allantoin was not influenced by oxidative stress metabolites as uric acid and 8-OHdG.

Overall, this work demonstrates the plasticity of design and analytical performance of integrating biopolymers, imprinting technology and structural coloration in an electrochemical device and opens exciting avenues for dual-signal biosensors for disease diagnosis.

CRediT authorship contribution statement

Akmaral Suleimenova: Writing – review & editing, Writing – original draft, Visualization, Validation, Methodology, Investigation, Data curation. **Ana C. Marques:** Writing – original draft, Methodology, Investigation. **Manuela F. Frasco:** Writing – review & editing, Visualization, Supervision, Methodology, Formal analysis, Data curation. **Elvira Fortunato:** Writing – review & editing, Supervision, Resources. **M. Goreti F. Sales:** Writing – review & editing, Supervision, Methodology, Funding acquisition, Conceptualization.

Declaration of competing interest

The authors declare that they have no known competing financial interests or personal relationships that could have appeared to influence the work reported in this paper.

Acknowledgements

The authors gratefully acknowledge funding from the European Commission through the project MindGAP (FET-Open/H2020/GA829040). This research was sponsored by national funds through FCT – Fundação para a Ciência e a Tecnologia, under projects UID/00285-Centre for Mechanical Engineering, Materials and Processes and LA/P/0112/2020. The author AS acknowledges the MIT-Portugal PhD grant PD/BD/142776/2018 funded by FCT.

Supplementary materials

Supplementary material associated with this article can be found, in the online version, at doi:10.1016/j.electacta.2025.146718.

Data availability

Data will be made available on request.

References

[1] H. Eynaki, M.Ali Kiani, H. Golmohammadi, Nanopaper-based screen-printed electrodes: a hybrid sensing bioplatform for dual opto-electrochemical sensing applications, Nanoscale 12 (35) (2020) 18409–18417, https://doi.org/10.1039/D0NR03505J.
[2] Y. Du, Z. Ke, J. Zhang, G. Feng, Dual-signal output paper sensor based on coordinative self-assembly biomimetic nanozyme for point-of-care detection of biomarker, Biosens. Bioelectron. 216 (Nov. 2022) 114656, https://doi.org/10.1016/j.bios.2022.114656.
[3] A. Ke, C. Li, B. Dong, X. Zhang, Biomimetic photonic crystal double-network hydrogel for visual and electrical dual signals bluetooth-enabled wearable sensor, J. Mater. Chem. C. (Apr. 2024), https://doi.org/10.1039/D4TC00998C.
[4] C. Fenzl, T. Hirsch, O.S. Wolfbeis, Photonic crystals for chemical sensing and biosensing, Angew. Chem. Int. Ed. 53 (13) (2014) 3318–3335, https://doi.org/10.1002/anie.201307828.
[5] H. Inan, et al., Photonic crystals: emerging biosensors and their promise for point-of-care applications, Chem. Soc. Rev. 46 (2) (Jan. 2017) 366–388, https://doi.org/10.1039/C6CS00206D.
[6] K. Li, C. Li, H. Li, M. Li, Y. Song, Designable structural coloration by colloidal particle assembly: from nature to artificial manufacturing, iScience 24 (2) (Feb. 2021) 102121, https://doi.org/10.1016/j.isci.2021.102121.
[7] N.S. Ergang, J.C. Lytle, K.T. Lee, S.M. Oh, W.H. Smyrl, A. Stein, Photonic crystal structures as a basis for a three-dimensionally interpenetrating electrochemical-cell system, Adv. Mater. 18 (13) (2006) 1750–1753, https://doi.org/10.1002/adma.200600295.
[8] H.B. Yildiz, B.B. Carbas, S. Sonmezoglu, M. Karaman, L. Toppare, A photoelectrochemical device for water splitting using oligoaniline-crosslinked [Ru(bpy)2(bpyCONHArNH2)]+2 dye/IrO2 nanoparticle array on TiO2 photonic crystal modified electrode, Int. J. Hydrog. Energy 41 (33) (Sep. 2016) 14615–14629, https://doi.org/10.1016/j.ijhydene.2016.04.249.
[9] M. Gugole, et al., High-contrast switching of plasmonic structural colors: inorganic versus organic electrochromism, ACS Photonics 7 (7) (Jul. 2020) 1762–1772, https://doi.org/10.1021/acsphotonics.0c00394.
[10] O. Olsson, M. Gugole, A. Dahlin, Enhanced electrochromic switching contrast in the blue by 3,4-propylenedioxypyrrole– implementation on structural colors, Nanophotonics 12 (8) (Apr. 2023) 1591–1599, https://doi.org/10.1515/nanoph-2022-0624.
[11] E.P. Chan, J.J. Walish, A.M. Urbas, E.L. Thomas, Mechanochromic photonic gels, Adv. Mater. 25 (29) (2013) 3934–3947, https://doi.org/10.1002/adma.201300692.
[12] H. Wang, H. Zhang, Z. Chen, Y. Zhao, Z. Gu, L. Shang, Polymer-based responsive structural color materials, Prog. Mater. Sci. 135 (Jun. 2023) 101091, https://doi.org/10.1016/j.pmatsci.2023.101091.
[13] J.C. Yang, J.Y. Park, Surface imprinted conducting polymer patterns electrochemically grown from gold pinhole arrays on 2D inverse silica opals and their effective use in aspartame detection, Sens. Actuators B: Chem. 255 (Feb. 2018) 463–470, https://doi.org/10.1016/j.snb.2017.08.097.
[14] M.A. Zoubi, R. Al-Salman, Y. Li, F. Endres, Highly ordered 3D-macroporous poly (Para-Phenylene) films made by electropolymerization of benzene in an ionic liquid, Z. Phys. Chem. 225 (4) (Apr. 2011) 393–403, https://doi.org/10.1524/zpch.2011.0091.
[15] T.S. Bedwell, M.J. Whitcombe, Analytical applications of MIPs in diagnostic assays: future perspectives, Anal Bioanal. Chem. 408 (7) (Mar. 2016) 1735–1751, https://doi.org/10.1007/s00216-015-9137-9.
[16] M.K.Nayak Disha, P. Kumari, M.K. Patel, P. Kumar, Functional nanomaterials based opto-electrochemical sensors for the detection of gonadal steroid hormones, TrAC Trends Anal. Chem. 150 (May 2022) 116571, https://doi.org/10.1016/j.trac.2022.116571.
[17] L. Chen, X. Wang, W. Lu, X. Wu, J. Li, Molecular imprinting: perspectives and applications, Chem. Soc. Rev. 45 (8) (Apr. 2016) 2137–2211, https://doi.org/10.1039/C6CS00061D.
[18] G. Ertürk, B. Mattiasson, Molecular imprinting techniques used for the preparation of biosensors, Sensors 17 (2) (Feb. 2017), https://doi.org/10.3390/s17020288. Art. no. 2.
[19] J. Wackerlig, P.A. Lieberzeit, Molecularly imprinted polymer nanoparticles in chemical sensing – Synthesis, characterisation and application, Sens. Actuators B: Chem. 207 (Feb. 2015) 144–157, https://doi.org/10.1016/j.snb.2014.09.094.
[20] L. Wang, M. Pagett, W. Zhang, Molecularly imprinted polymer (MIP) based electrochemical sensors and their recent advances in health applications, Sens. Actuators Rep. 5 (Jun. 2023) 100153, https://doi.org/10.1016/j.snr.2023.100153.
[21] Q. Han, C. Wang, P. Liu, G. Zhang, L. Song, Y. Fu, Achieving synergistically enhanced dual-mode electrochemiluminescent and electrochemical drug sensors via a multi-effect porphyrin-based metal-organic framework, Sens. Actuators B: Chem. 330 (Mar. 2021) 129388, https://doi.org/10.1016/j.snb.2020.129388.
[22] B. Lenyk, et al., Dual-transducer malaria aptasensor combining electrochemical impedance and surface plasmon polariton detection on gold nanohole arrays, Chem. Electro. Chem. 7 (22) (2020) 4594–4600, https://doi.org/10.1002/celc.202001212.
[23] R. Zhu, et al., A combined plasmonic and electrochemical aptasensor based on gold nanopit arrays for the detection of Human serum albumin, Nanomaterials 13 (16) (Jan. 2023), https://doi.org/10.3390/nano13162374. Art. no. 16.
[24] D. Il'yasova, et al., Urinary biomarkers of oxidative status in a clinical model of oxidative assault, Cancer Epidemiol Biomark. Prev. 19 (6) (Jun. 2010) 1506–1510, https://doi.org/10.1158/1055-9965.EPI-10-0211.

[25] R. Kand'ár, P. Záková, Allantoin as a marker of oxidative stress in human erythrocytes, Clin. Chem. Lab. Med. 46 (9) (2008) 1270–1274, https://doi.org/10.1515/CCLM.2008.244.
[26] M.-P. Martinez-Moral, K. Kannan, Allantoin as a marker of oxidative stress: inter- and intraindividual variability in urinary concentrations in healthy individuals, Env.. Sci. Technol. Lett. 6 (5) (May 2019) 283–288, https://doi.org/10.1021/acs.estlett.9b00142.
[27] M. Saqib, B. Lou, M.I. Halawa, S.A. Kitte, Z. Liu, G. Xu, Chemiluminescence of Lucigenin–Allantoin and its application for the detection of Allantoin, Anal. Chem. 89 (3) (Feb. 2017) 1863–1869, https://doi.org/10.1021/acs.analchem.6b04271.
[28] K.M. Kim, et al., Simultaneous determination of uric acid metabolites allantoin, 6-aminouracil, and triuret in human urine using liquid chromatography-mass spectrometry, J. Chromatogr. B Anal. Technol. Biomed. Life Sci. 877 (1–2) (Jan. 2009) 65–70, https://doi.org/10.1016/j.jchromb.2008.11.029.
[29] A.A. Tolun, H. Zhang, D. Il'yasova, J. Sztáray, S.P. Young, D.S. Millington, Allantoin in human urine quantified by ultra-performance liquid chromatography-tandem mass spectrometry, Anal. Biochem. 402 (2) (Jul. 2010) 191–193, https://doi.org/10.1016/j.ab.2010.03.033.
[30] R. Turner, L.K. Stamp, A.J. Kettle, Detection of allantoin in clinical samples using hydrophilic liquid chromatography with stable isotope dilution negative ion tandem mass spectrometry, J. Chromatogr. B Anal. Technol. Biomed. Life Sci. 891–892 (Apr. 2012) 85–89, https://doi.org/10.1016/j.jchromb.2012.02.009.
[31] E.B. Aydın, M.K. Sezgintürk, Indium tin oxide (ITO): A promising material in biosensing technology, TrAC Trends Anal. Chem. 97 (Dec. 2017) 309–315, https://doi.org/10.1016/j.trac.2017.09.021.
[32] H. Silah, C. Erkmen, E. Demir, B. Uslu, Modified indium tin oxide electrodes: electrochemical applications in pharmaceutical, biological, environmental and food analysis, TrAC Trends Anal. Chem. 141 (Aug. 2021) 116289, https://doi.org/10.1016/j.trac.2021.116289.
[33] Y. Jiang, et al., Polydopamine-based photonic crystal structures, J. Mater. Chem. C. 1 (38) (Sep. 2013) 6136–6144, https://doi.org/10.1039/C3TC30114A.
[34] M. Kohri, Progress in polydopamine-based melanin mimetic materials for structural color generation, Sci. Technol. Adv. Mater. (Jan. 2020). Accessed: Apr. 26, 2024 [Online]. Available: https://www.tandfonline.com/doi/abs/10.1080/14686996.2020.1852057.
[35] M.E. Lynge, R. Van Der Westen, A. Postma, B. Städler, Polydopamine—a nature-inspired polymer coating for biomedical science, Nanoscale 3 (12) (Dec. 2011) 4916–4928, https://doi.org/10.1039/C1NR10969C.
[36] P. Palladino, F. Bettazzi, S. Scarano, Polydopamine: surface coating, molecular imprinting, and electrochemistry—Successful applications and future perspectives in (bio)analysis, Anal. Bioanal. Chem. 411 (19) (Jul. 2019) 4327–4338, https://doi.org/10.1007/s00216-019-01665-w.
[37] Z. Xia, et al., Facile synthesis of polydopamine-coated molecularly imprinted silica nanoparticles for protein recognition and separation, Biosens. Bioelectron. 47 (Sep. 2013) 120–126, https://doi.org/10.1016/j.bios.2013.03.024.
[38] W. Stöber, A. Fink, E. Bohn, Controlled growth of monodisperse silica spheres in the micron size range, J. Colloid Interface Sci. 26 (1) (Jan. 1968) 62–69, https://doi.org/10.1016/0021-9797(68)90272-5.
[39] S.H. Yalkowsky, Y. He, P. Jain, Handbook of Aqueous Solubility Data, 2nd ed., CRC Press, Boca Raton, 2010 https://doi.org/10.1201/EBK1439802458.
[40] T. Brooks, C.W. Keevil, A simple artificial urine for the growth of urinary pathogens, Lett. Appl. Microbiol. 24 (3) (Mar. 1997) 203–206, https://doi.org/10.1046/j.1472-765x.1997.00378.x.
[41] D. Giavarina, Understanding Bland Altman analysis, Biochem. Med. 25 (2) (Jun. 2015) 141–151, https://doi.org/10.11613/BM.2015.015.
[42] T. Jung, et al., Automated determination of 8-OHdG in cells and tissue via immunofluorescence using a specially created antibody, Biotechnol. Rep. 42 (Jun. 2024) e00833, https://doi.org/10.1016/j.btre.2024.e00833.
[43] M. Kopčil, R. Kanďár, Screening method for the simultaneous determination of allantoin and uric acid from dried blood spots, J. Pharm. Biomed. Anal. 225 (Feb. 2023) 115222, https://doi.org/10.1016/j.jpba.2022.115222.
[44] K. Orfanakos, et al., The predictive value of 8-hydroxy-deoxyguanosine (8-OHdG) serum concentrations in irradiated non-small cell lung carcinoma (NSCLC) patients, Biomedicines 12 (1) (Jan. 2024), https://doi.org/10.3390/biomedicines12010134. Art. no. 1.
[45] Y.Y. Sautin, R.J. Johnson, Uric acid: the oxidant-antioxidant paradox, Nucleosides Nucleotides Nucleic. Acids. 27 (6) (Jun. 2008) 608–619, https://doi.org/10.1080/15257770802138558.
[46] R.P. Buck, E. Lindner, Recommendations for nomenclature of ionselective electrodes (IUPAC Recommendations 1994), Pure. Appl. Chem. 66 (12) (Jan. 1994) 2527–2536, https://doi.org/10.1351/pac199466122527.
[47] M.T. Dang, J. Lefebvre, J.D. Wuest, Recycling indium tin oxide (ITO) electrodes used in thin-film devices with adjacent hole-transport layers of metal oxides, ACS Sustain. Chem. Eng. 3 (12) (2015) 3373–3381, https://doi.org/10.1021/acssuschemeng.5b01080.
[48] A. Minenkov, S. Hollweger, J. Duchoslav, O. Erdene-Ochir, M. Weise, E. Ermilova, A. Hertwig, M. Schiek, Monitoring the electrochemical failure of indium tin oxide electrodes via operando ellipsometry complemented by electron microscopy and spectroscopy, ACS Appl. Mater. Interfac. 16 (7) (2024) 9517–9531, https://doi.org/10.1021/acsami.3c17923.
[49] J. Szewczyk, D. Aguilar-Ferrer, E. Coy, Polydopamine films: electrochemical growth and sensing applications, Eur. Polym. J. 174 (Jul. 2022) 111346, https://doi.org/10.1016/j.eurpolymj.2022.111346.
[50] E.S.A. Goerlitzer, R.N. Klupp Taylor, N. Vogel, Bioinspired photonic pigments from colloidal self-assembly, Adv. Mater. 30 (28) (2018) 1706654, https://doi.org/10.1002/adma.201706654.
[51] G.K. Glantzounis, E.C. Tsimoyiannis, A.M. Kappas, D.A. Galaris, Uric acid and oxidative stress, Curr. Pharm. Des. 11 (32) (2005) 4145–4151, https://doi.org/10.2174/138161205774913255.
[52] M. Graille, P. Wild, J.-J. Sauvain, M. Hemmendinger, I.Guseva Canu, N.B. Hopf, Urinary 8-OHdG as a biomarker for oxidative stress: a systematic literature review and meta-analysis, Int. J. Mol. Sci. 21 (11) (Jan. 2020), https://doi.org/10.3390/ijms21113743 no. 11, Art. no.